

We are IntechOpen, the world's leading publisher of Open Access books Built by scientists, for scientists

6,900

Open access books available

186,000

International authors and editors

200M

Downloads

Our authors are among the

154

Countries delivered to

TOP 1%

most cited scientists

12.2%

Contributors from top 500 universities



WEB OF SCIENCE™

Selection of our books indexed in the Book Citation Index
in Web of Science™ Core Collection (BKCI)

Interested in publishing with us?
Contact book.department@intechopen.com

Numbers displayed above are based on latest data collected.
For more information visit www.intechopen.com



Nematicity in Electron-Doped Iron-Pnictide Superconductors

Hong-Yi Chen

Abstract

The nature of the nematicity in iron pnictides is studied with a proposed magnetic fluctuation. The spin-driven order in the iron-based superconductor has been realized in two categories: stripe SDW state and nematic state. The stripe SDW order opens a gap in the band structure and causes a deformed Fermi surface. The nematic order does not make any gap in the band structure and still deforms the Fermi surface. The electronic mechanism of nematicity is discussed in an effective model by solving the self-consistent Bogoliubov-de Gennes equations. The nematic order can be visualized as crisscross horizontal and vertical stripes. Both stripes have the same period with different magnitudes. The appearance of the orthorhombic magnetic fluctuations generates two uneven pairs of peaks at $(\pm\pi, 0)$ and $(0, \pm\pi)$ in its Fourier transformation. In addition, the nematic order breaks the degeneracy of d_{xz} and d_{yz} orbitals and causes the elliptic Fermi surface near the Γ point. The spatial image of the local density of states reveals a $d_{x^2-y^2}$ -symmetry form factor density wave.

Keywords: magnetic fluctuation, stripe SDW, nematic order, two-orbital, elliptic Fermi surface, LDOS maps

1. Introduction

The discovery of Fe-based superconductors with critical temperatures up to 55 K has begun a new era of investigations of the unconventional superconductivity. In common with copper-like superconductors (cuprate), the emergence of superconductivity in electron-doped Fe-pnictides such as $\text{Ba}(\text{Fe}_{1-x}\text{Co}_x\text{As})_2$ is to suppress the magnetic order and fluctuations originated in the parent compound with $x = 0$ [1]. The intertwined phases between the superconductivity and stripe spin density wave (SDW) order (ferromagnetic stripes along one Fe-Fe bond direction that is antiferromagnetically aligned along orthogonal Fe—Fe bond) are of particular interests. In both pnictides and cuprates, the experimentally observed nematicity exists in an exotic phase between the superconductivity (SC) and the stripe SDW [2]. The nematicity occurs in weakly doped iron pnictides with tetragonal-to-orthorhombic structural transition [3–17], i.e., in a square unit cell, the point-group symmetry is reduced from C_4 (tetragonal) to C_2 (orthorhombic).

At present, there are two scenarios for the development of nematic order through the electronic configurations [18]. One scenario is the orbital fluctuations [19–23]. The structural order is driven by orbital ordering. The orbital ordering induces magnetic anisotropy and triggers the magnetic transition at a lower

temperature. The other scenario is the spin fluctuation [24–27]. The magnetic mechanism for the structural order is associated with the onset of SDW.

Recently, Lu et al. [28] reported that the low-energy spin fluctuation excitations in underdoped sample $\text{BaFe}_{1.915}\text{Ni}_{0.085}\text{As}_2$ change from C_4 symmetry to C_2 symmetry in the nematic state. Zhang et al. [29] exhibited that the reduction of the spin-spin correlation length at $(0, \pi)$ in $\text{BaFe}_{1.935}\text{Ni}_{0.065}\text{As}_2$ happens just below T_s , suggesting the strong effect of nematic order on low-energy spin fluctuations. Apparently, these experiments above have provided a spin-driven nematicity picture.

The partial melting of SDW has been proposed as the mechanism to explain the nematicity. The properties of the spin-driven nematic order have been studied in Landau-Ginzburg-Wilson's theory [18, 24–26]. Meanwhile, the lack of the realistic microscopic model is responsible for the debates where the leading electronic instability, i.e., the onset of SDW, causes the nematic order. Recently, an extended random phase approximation (RPA) approach in a five-orbital Hubbard model including Hund's rule interaction has shown that the leading instability is the SDW-driven nematic phase [30]. Although the establishment of the nematicity in the normal state has attracted a lot of attentions, the microscopic description of the nematic order and, particularly, the relation between SC and the nematic order are still missing.

The magnetic mechanism for the structural order is usually referred to the Ising-nematic phase where stripe SDW order can be along the x-axis or the y-axis. The nematic phase is characterized by an underlying electronic order that the Z_2 symmetry between the x- and y- directions is broken above and the $O(3)$ spin-rotational symmetry is preserved [25].

The magnetic configuration in FeSCs can be described in terms of two magnetic order parameters Δ_x and Δ_y . Both order parameters conventionally defined in momentum space are written as

$$\Delta_\ell = \sum_k c_{k+Q_\ell, \alpha}^\dagger \sigma_{\alpha\beta} c_{k, \beta}, \quad (1)$$

where $\ell = x$ or y . Here the wave vectors $Q_x = (\pi, 0)$ and $Q_y = (0, \pi)$ correspond to the spins parallel along the y-axis and antiparallel along the x-axis and the spins parallel along the x-axis and antiparallel along the y-axis, respectively.

In the stripe SDW state, the order parameters are set to $\langle \Delta_x \rangle \neq 0$ or $\langle \Delta_y \rangle \neq 0$, i.e., $\langle \Delta_\ell \rangle \neq 0$. This implies to choose an ordering vector either Q_x or Q_y . The Z_2 symmetry indicating to the degenerate of spin stripes along the y-axis (corresponding to Q_x) or x-axis (corresponding to Q_y) is broken. In addition, the $O(3)$ spin-rotational symmetry is also broken. In the real space configuration, the magnetic ground state is an orthorhombic uniaxial stripe state. The stripe order reduces the point-group symmetry of a unit cell from C_4 (tetragonal) to C_2 (orthorhombic). In the nematic state, the order parameters are set to $\langle \Delta_x \rangle = \langle \Delta_y \rangle = 0$ and $\langle \Delta_x^2 \rangle \neq \langle \Delta_y^2 \rangle$. This implies that the magnetic fluctuations associated with one of the ordering vectors are stronger than the other $\langle \Delta_x^2 \rangle > \langle \Delta_y^2 \rangle$ or $\langle \Delta_y^2 \rangle > \langle \Delta_x^2 \rangle$. Therefore, the Z_2 symmetry is broken, but the $O(3)$ spin-rotational symmetry is not. In the real space configuration, the x- and y-directions of the magnetic fluctuations are inequivalent.

Recently, the reentrant C_4 symmetry magnetic orders have been reported in hole-doped Fe-pnictide [27, 31, 32]. A double-Q order (choose both Q_x and Q_y) has been proposed to change the ground state from striped to tetragonal [33, 34].

Two stripe orders with the ordering vectors Q_x and Q_y are superposed to preserve the tetragonal symmetry. As a matter of fact, the nematic phase is characterized by an underlying electronic order that spontaneously breaks tetragonal symmetry. Since the double-Q order does not break the C_4 symmetry, it is not suitable to explain the nematicity.

The magnetic fluctuations trigger a transition from the tetragonal-to-orthorhombic phase. At very high temperature, $T > T_S$, $\langle \Delta_x \rangle = \langle \Delta_y \rangle = 0$, and the fluctuations of all order parameters have equal strength, i.e., $\langle \Delta_x^2 \rangle = \langle \Delta_y^2 \rangle$. As the temperature lowers, $T_N < T < T_S$, the thermodynamic average of order parameters still remains $\langle \Delta_x \rangle = \langle \Delta_y \rangle = 0$ but $\langle \Delta_x^2 \rangle \neq \langle \Delta_y^2 \rangle$. The fluctuations of one of the orders Δ_x are on average different from the fluctuations of the other order Δ_y , implying a broken Z_2 symmetry and a preserved $O(3)$ symmetry. When the temperature is below T_N , the magnetic ground state is a stripe SDW state, i.e., $\langle \Delta_x \rangle = 0$ or $\langle \Delta_y \rangle = 0$.

In this chapter, we will exploit a two-orbital model to study the interplay between SC and nematicity in a two-dimensional lattice. The two-orbital model has been successfully used in many studies such as quasiparticle excitation, the density of states near an impurity [35, 36] and the magnetic structure of a vortex core [37].

2. Model

Superconductivity in the iron-pnictide superconductors originates from the FeAs layer. The Fe atoms form a square lattice, and the As atoms are alternatively above and below the Fe-Fe plane. This leads to two sublattices of irons denoted by sublattices A and B. Many tight-binding Hamiltonians have been proposed to study the electronic band structure that includes five Fe 3d orbitals [38], three Fe orbitals [39, 40], and simply two Fe bands [41–43]. Each of these models has its own advantages and range of convenience for calculations. For example, the five-orbital tight-binding model can capture all details of the DFT bands across the Fermi energy in the first Brillouin zone. However, in practice, it becomes a formidable task to solve the Hamiltonian with a large size of lattice in real space even in the mean-field level. Several studies used five-orbital models in momentum space to investigate the single-impurity problem for different iron-based compounds such as $\text{LaFeAsO}_{1-x}\text{F}_x$, LiFeAs , and $\text{K}_x\text{Fe}_{2-y}\text{Se}_2$. These studies confirmed that the detail of electronic bands strongly influences on the magnitude and location of the in-gap resonant states generated by the scattering of quasiparticles from single impurity [44–46].

On the other hand, the two-orbital models apparently have a numerical advantage dealing with a large size of lattice while retaining some of the orbital characters of the low-energy bands. Among the two-orbital (d_{xz} and d_{yz}) models, Zhang [47] proposed a phenomenological approach to take into account the two Fe atoms per unit cell and the asymmetry of the As atoms below and above of the Fe plane. Later on, Tai and co-workers [48] improved Zhang's model by a phenomenological two-by-two-orbital model (two Fe sites with two orbitals each). The obtained low-energy electronic dispersion agrees qualitatively well with DFT in LDA calculations of the entire Brillouin zone of the 122 compounds.

The multi-orbital Hamiltonian of the iron-pnictide superconductors in a two-dimensional square lattice is described as

$$\begin{aligned}
 H = & \sum_{ijuv\alpha} t_{ijuv} c_{iua}^\dagger c_{jv\alpha} - \mu \sum_{iua} n_{iua} + U \sum_{iu} n_{iu\uparrow} n_{iu\downarrow} + \left(U' - \frac{J_H}{2} \right) \sum_{i, u < v, \alpha\beta} n_{iua} n_{iv\beta} \\
 & - 2J_H \sum_{i, u < v} S_{iu} \cdot S_{iv} + J' \sum_{i, u \neq v} c_{iu\uparrow}^\dagger c_{iu\downarrow}^\dagger c_{iv\downarrow} c_{iv\uparrow},
 \end{aligned} \quad (2)$$

where

$$n_{iua} = c_{iua}^\dagger c_{iua}, \quad (3)$$

$$S_{iu} = \frac{1}{2} \sum_{\alpha\beta} c_{iua}^\dagger \sigma_{\alpha\beta} c_{iub}, \quad (4)$$

with $\sigma_{\alpha\beta}$ the Pauli matrices. The operators c_{iua}^\dagger (c_{iua}) create (annihilate) an electron with spin $\alpha, \beta = \uparrow, \downarrow$ in the orbital $u, v = 1, 2$ on the lattice site i ; t_{ijuv} is the hopping matrix element between the neighbor sites, and μ is the chemical potential. U (U') is the intraorbital (interorbital) on-site interaction. Hund's rule coupling is J_H and the pair hopping energy is J' . The spin-rotation invariance gives $U' = U - 2J_H$ and $J' = J_H$ [49]. Repulsion between electrons requires $J_H < U/3$.

Here, we adopt Tai's phenomenological two-by-two-orbital model because it is able to deal with a large size of lattice in many aspects and the details of low-energy bands are similar to the results from DFT + LDA. In a two-orbital model, the hopping amplitudes are chosen as shown in **Figure 1** [48] to fit the band structure from the first-principle calculations:

$$t_1 = t_{i, i \pm x(y), u, u} = -1, \quad (5)$$

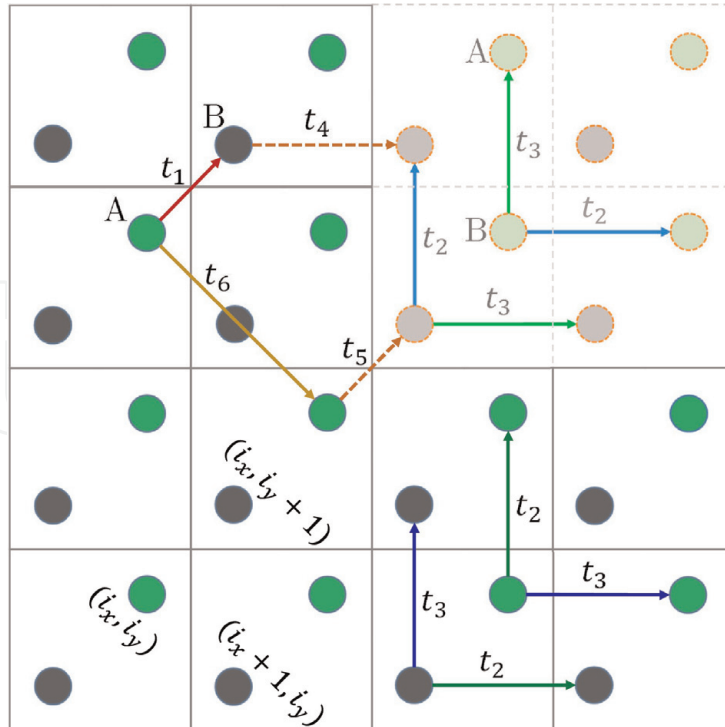


Figure 1.

(color online) two-dimensional square lattice of the iron-based superconductors. There are two Fe atoms (green and gray color) in a unit cell, and each atom has two orbitals. The bright color circle represents the first orbital, and the faded color circle represents the second orbital. Solid lines indicate the hopping between the atoms in the same orbital and dashed lines indicate the hopping between the atoms in the different orbitals.

$$\left\{ \begin{array}{l} \frac{1 + (-1)^{x+y+u}}{2} t_2 + \frac{1 - (-1)^{x+y+u}}{2} t_3 = t_{i, i\pm(x+y), u, u} = 0.08 \\ \frac{1 + (-1)^{x-y+u}}{2} t_3 + \frac{1 - (-1)^{x-y+u}}{2} t_2 = t_{i, i\pm(x-y), u, u} = 1.35 \end{array} \right. , \quad (6)$$

$$t_4 = t_{i, i\pm(x\pm y), u, v\neq u} = -0.12, \quad (7)$$

$$t_5 = t_{i, i\pm x(y), u, v\neq u} = 0.09, \quad (8)$$

$$t_6 = t_{i, i\pm 2x(2y), u, u} = 0.25, \quad (9)$$

where $u \neq v$ indicates two different orbitals.

Figure 1 shows the hopping parameters between unit cells and orbitals. For the same orbital, the hopping parameters t_2 and t_3 are chosen differently along the mutually perpendicular directions. The C_4 symmetry on the same orbital between different sublattices is broken. However, t_2 and t_3 are twisted for the different Fe atoms on the same sublattice which restore the C_4 symmetry of the lattice structure.

In the mean-field level

$$H = H_0 + H_\Delta + H_{\text{int}}, \quad (10)$$

the Hamiltonian is self-consistently solved accompanied with s^{+-} -wave superconducting order. The mean-field scheme is the same as Ref. [48]:

$$H_0 = \sum_{ijv\alpha} t_{ijv} c_{i\alpha}^\dagger c_{jv\alpha} - \mu \sum_{i\alpha} n_{i\alpha}, \quad (11)$$

$$H_\Delta = \sum_{ij\alpha\beta} \left(\Delta_{ij\alpha} c_{i\alpha}^\dagger c_{j\beta}^\dagger + \text{h.c.} \right), \quad (12)$$

$$H_{\text{int}} = U \sum_{iu, \alpha \neq \beta} \langle n_{iu\beta} \rangle n_{iu\alpha} + U' \sum_{i, u < v, \alpha \neq \beta} \langle n_{iu\beta} \rangle n_{iv\alpha} + (U' - J_H) \sum_{i, u < v, \alpha} \langle n_{iu\alpha} \rangle n_{iv\alpha}. \quad (13)$$

The next nearest-neighbor intraorbital attractive interaction V is responsible for the superconducting order parameter $\Delta_{ijuu} = V \langle c_{i\uparrow} c_{j\downarrow} \rangle$ [50–52]. According to the literatures where U is chosen to be 3.2 or less [48, 52], the magnetic configuration is a uniform SDW order. In order to make the stripe SDW order and the nematic order by changing electron doping, i.e., the chemical potential μ , we choose the parameters of interactions $U = 3.5$, $J_H = 0.4$, and $V = 1.3$ to induce a nematic order within a small doping range.

In momentum space, the spin configuration is determined by the order parameters Δ_x and Δ_y . The combination of these order parameters lacks the visualization of the magnetic structure in real space. Therefore, we choose the staggered magnetization M_i in a lattice to study the states driven by the magnetic mechanism. The magnetic configuration is described as

$$M_i = M_1 \cos(q_y \cdot r_i) e^{iQ_x \cdot r_i} + M_2 \sin(q_x \cdot r_i) e^{iQ_y \cdot r_i}, \quad (14)$$

where the wave vectors $q_x = (2\pi/\lambda, 0)$ and $q_y = (0, 2\pi/\lambda)$ correspond to a modulation along the x-axis and the y-axis with wavelength λ . M_1 and M_2 are the amplitude of the modulation.

In the case of the absence of both q_x and q_y , M_i becomes

$$M_i = M_1 e^{iQ_x r_i} + M_2 e^{iQ_y r_i}. \quad (15)$$

As $M_1 = 0$ or $M_2 = 0$ is chosen, i.e., choosing the ordering vector either Q_x or Q_y , the state is a stripe SDW state. The existence of q_x and q_y does not affect the stripe SDW state. As two values of M_1 and M_2 are arbitrarily chosen, the spin configuration forms a stripe SDW along the (1, 1) direction. The existence of q_x and q_y has a lot of influences on the nematic state.

In the nematic state, the presence of both Q and q ordering vectors is necessary. Unlike the double-Q model, with the choice $M_1 \neq M_2$, the magnitudes of the modulated antiparallel spins along the x-axis and the y-axis are different due to the existence of q vectors. The magnetic configuration is attributed to two inequivalent stripes interpenetrating each other and formed a checked pattern. The checked pattern has the same period along the x- and y-directions. The period is determined by the value of q in the periodic boundary conditions. The value of q , therefore, cannot be arbitrary and must commensurate the lattice to stabilize the modulation and lower the energy of the system. As two modulated stripes have no phase difference, the checked pattern shows a s -wave-like symmetry. In addition, as the modulations have a phase shift of $\pi/2$, the checked pattern shows a d -wave-like symmetry.

Figure 2 displays the Fermi surface and the band structure in the absence of SDW at the normal state, i.e., the superconductivity is set to zero. In the absence of SDW ($U = 0$), the Hamiltonian in momentum space is

$$\Psi^\dagger = (c_{A1k\sigma}^\dagger \ c_{A2k\sigma}^\dagger \ c_{B1k\sigma}^\dagger \ c_{B2k\sigma}^\dagger), \quad (16)$$

$$H_0 = \sum_{k\sigma} \Psi^\dagger \begin{pmatrix} \varepsilon_{A1} & \varepsilon_{12} & \varepsilon_{AB} & \varepsilon_c \\ \varepsilon_{12} & \varepsilon_{A2} & \varepsilon_c & \varepsilon_{AB} \\ \varepsilon_{AB} & \varepsilon_c & \varepsilon_{B1} & \varepsilon_{12} \\ \varepsilon_c & \varepsilon_{AB} & \varepsilon_{12} & \varepsilon_{B2} \end{pmatrix} \Psi, \quad (17)$$

where

$$\varepsilon_{A1} = -2t_3 \cos k_x - 2t_2 \cos k_y - 4t_6 \cos k_x \cos k_y, \quad (18)$$

$$\varepsilon_{A2} = -2t_2 \cos k_x - 2t_3 \cos k_y - 4t_6 \cos k_x \cos k_y, \quad (19)$$

$$\varepsilon_{B1} = -2t_2 \cos k_x - 2t_3 \cos k_y - 4t_6 \cos k_x \cos k_y, \quad (20)$$

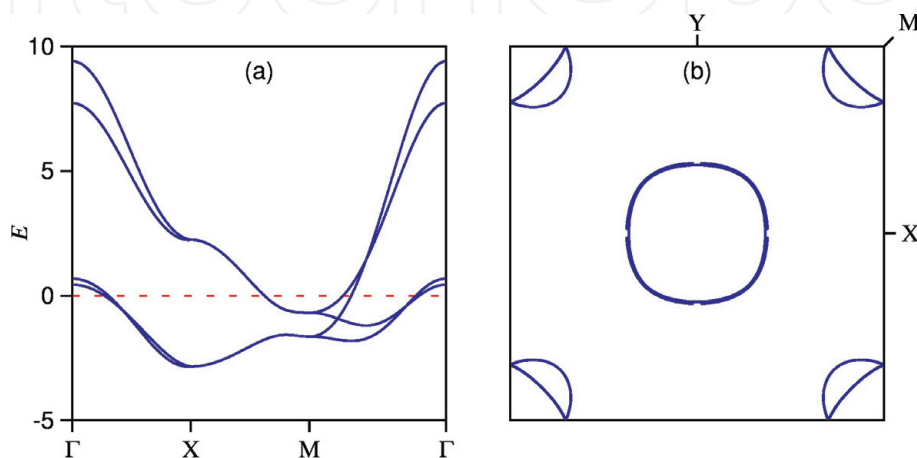


Figure 2. (color online) (a) and (b) are, respectively, the band structure and the Fermi surface without SDW. The Fermi energy (red dashed line) corresponds to the electron filling $n = 2.1$.

$$\varepsilon_{B2} = -2t_3 \cos k_x - 2t_2 \cos k_y - 4t_6 \cos k_x \cos k_y, \quad (21)$$

$$\varepsilon_{12} = t - 2t_4 \cos k_x - 2t_4 \cos k_y, \quad (22)$$

$$\varepsilon_{AB} = -4t_1 \cos \frac{k_x}{2} \cos \frac{k_y}{2}, \quad (23)$$

$$\varepsilon_c = -4t_5 \cos \frac{k_x}{2} \cos \frac{k_y}{2}. \quad (24)$$

The eigenvalues are

$$E_{1,k} = \bar{\varepsilon}_+ - \sqrt{\bar{\varepsilon}_-^2 + (\varepsilon_{12} - \varepsilon_{AB})^2} - \varepsilon_c - \mu, \quad (25)$$

$$E_{2,k} = \bar{\varepsilon}_+ + \sqrt{\bar{\varepsilon}_-^2 + (\varepsilon_{12} - \varepsilon_{AB})^2} - \varepsilon_c - \mu, \quad (26)$$

$$E_{3,k} = \bar{\varepsilon}_+ - \sqrt{\bar{\varepsilon}_-^2 + (\varepsilon_{12} + \varepsilon_{AB})^2} + \varepsilon_c - \mu, \quad (27)$$

$$E_{4,k} = \bar{\varepsilon}_+ + \sqrt{\bar{\varepsilon}_-^2 + (\varepsilon_{12} + \varepsilon_{AB})^2} + \varepsilon_c - \mu, \quad (28)$$

where

$$\bar{\varepsilon}_\pm = \frac{\varepsilon_{A1} \pm \varepsilon_{B1}}{2}. \quad (29)$$

Figure 2(a) shows that two hole bands are around the Γ point and two electron bands are around the M point. There is no gap in the band structure where the superconductivity is able to open a gap. The nature of Fermi surface is revealed by the line at the Fermi energy crossing the band dispersion through $\Gamma - X - M - \Gamma$ points. **Figure 2(b)** displays that the Fermi surface contains two hole pockets that are centered at Γ point and two electron pockets that are centered at M points. In addition, the Fermi surface also exhibits the C_4 symmetry of the lattice structure.

In the stripe SDW state, the spin configuration is shown as **Figure 3**. The stripe SDW order enlarges the two-Fe unit cell to four-Fe unit cell as denoted by the blue

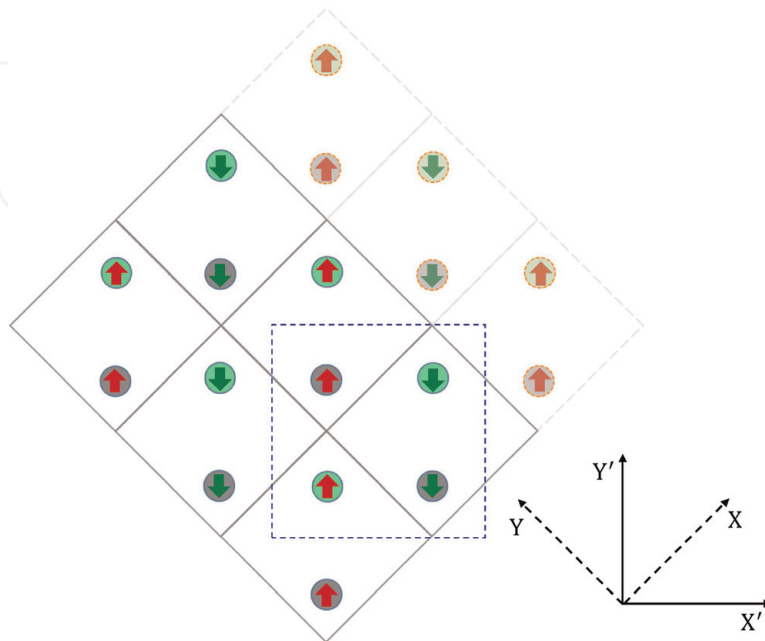


Figure 3. (color online) the schematic lattice structure of the Fe layer in the stripe SDW state. Blue dashed square denotes the four-Fe unit cell in the stripe SDW state.

dashed square in **Figure 3**. The antiferromagnetic order is along the X' -axis and the ferromagnetic order is along the Y' -axis. The magnetic unit cell (four-Fe unit cell) with lattice spacing $\sqrt{2}a$ is oriented at a 45° angle with respect to the non-magnetic unit cell (two-Fe unit cell). The magnetic Brillouin zone is a square oriented at a 45° angle with respect to the crystal Brillouin zone. The size of the magnetic unit cell is twice of the nonmagnetic unit cell, and the size of the magnetic Brillouin zone is half of the crystal Brillouin zone. The Hamiltonian in momentum space is

$$\tilde{\Psi}_k^\dagger = \left(c_{A_1^{(1)}k}^\dagger, c_{A_1^{(2)}k}^\dagger, c_{B_1^{(1)}k}^\dagger, c_{B_1^{(2)}k}^\dagger, c_{B_2^{(1)}k}^\dagger, c_{B_2^{(2)}k}^\dagger, c_{A_2^{(1)}k}^\dagger, c_{A_2^{(2)}k}^\dagger \right), \quad (30)$$

$$H = \sum_k \tilde{\Psi}_k^\dagger \cdot \mathbf{h} \cdot \tilde{\Psi}_k, \quad (31)$$

$$\mathbf{h} = \begin{pmatrix} \varepsilon_{A_1^1} & 0 & \varepsilon_{t_1^x} & \varepsilon_{t_5^x} & \varepsilon_{t_1^y} & \varepsilon_{t_5^y} & \varepsilon_{t_{23}} & \varepsilon_{t_4} \\ 0 & \varepsilon_{A_1^2} & \varepsilon_{t_5^x} & \varepsilon_{t_1^x} & \varepsilon_{t_5^y} & \varepsilon_{t_1^y} & \varepsilon_{t_4} & \varepsilon_{t_{32}} \\ \varepsilon_{t_1^x} & \varepsilon_{t_5^x} & \varepsilon_{B_1^1} & 0 & \varepsilon_{t_{32}} & \varepsilon_{t_4} & \varepsilon_{t_1^y} & \varepsilon_{t_5^y} \\ \varepsilon_{t_5^x} & \varepsilon_{t_1^x} & 0 & \varepsilon_{B_1^2} & \varepsilon_{t_4} & \varepsilon_{t_{23}} & \varepsilon_{t_5^y} & \varepsilon_{t_1^y} \\ \varepsilon_{t_1^y} & \varepsilon_{t_5^y} & \varepsilon_{t_{32}} & \varepsilon_{t_4} & \varepsilon_{B_2^1} & 0 & \varepsilon_{t_1^x} & \varepsilon_{t_5^x} \\ \varepsilon_{t_5^y} & \varepsilon_{t_1^y} & \varepsilon_{t_4} & \varepsilon_{t_{23}} & 0 & \varepsilon_{B_2^2} & \varepsilon_{t_5^x} & \varepsilon_{t_1^x} \\ \varepsilon_{t_{23}} & \varepsilon_{t_4} & \varepsilon_{t_1^y} & \varepsilon_{t_5^y} & \varepsilon_{t_1^x} & \varepsilon_{t_5^x} & \varepsilon_{A_2^1} & 0 \\ \varepsilon_{t_4} & \varepsilon_{t_{32}} & \varepsilon_{t_5^y} & \varepsilon_{t_1^y} & \varepsilon_{t_5^x} & \varepsilon_{t_1^x} & 0 & \varepsilon_{A_2^2} \end{pmatrix}, \quad (32)$$

where

$$\varepsilon_{t_1^x} = -2t_1 \cos k_x = -2t_1 \cos \left(\frac{k_{x'}}{\sqrt{2}} \right), \quad (33)$$

$$\varepsilon_{t_1^y} = -2t_1 \cos k_y = -2t_1 \cos \left(\frac{k_{y'}}{\sqrt{2}} \right), \quad (34)$$

$$\varepsilon_{t_5^x} = -2t_5 \cos k_x = -2t_5 \cos \left(\frac{k_{x'}}{\sqrt{2}} \right), \quad (35)$$

$$\varepsilon_{t_5^y} = -2t_5 \cos k_y = -2t_5 \cos \left(\frac{k_{y'}}{\sqrt{2}} \right), \quad (36)$$

$$\varepsilon_{t_{23}} = -2t_2 \cos(k_x + k_y) - 2t_3 \cos(k_x - k_y) = -2t_2 \cos \left(\frac{k_{x'} + k_{y'}}{\sqrt{2}} \right) - 2t_3 \cos \left(\frac{k_{x'} - k_{y'}}{\sqrt{2}} \right), \quad (37)$$

$$\varepsilon_{t_{32}} = -2t_3 \cos(k_x + k_y) - 2t_2 \cos(k_x - k_y) = -2t_3 \cos \left(\frac{k_{x'} + k_{y'}}{\sqrt{2}} \right) - 2t_2 \cos \left(\frac{k_{x'} - k_{y'}}{\sqrt{2}} \right), \quad (38)$$

$$\varepsilon_{t_4} = -2t_4 \cos(k_x + k_y) - 2t_4 \cos(k_x - k_y) = -4t_4 \cos \frac{k_{x'}}{\sqrt{2}} \cos \frac{k_{y'}}{\sqrt{2}}, \quad (39)$$

$$\varepsilon_{t_6} = -2t_6 \cos 2k_x - 2t_6 \cos 2k_y = -2t_6 \cos \sqrt{2}k_{x'} - 2t_6 \cos \sqrt{2}k_{y'} \quad (40)$$

$$\varepsilon_{A_1^1} = \varepsilon_{t_6} + U \langle n_{A_1^1 k \downarrow} \rangle + U' \langle n_{A_1^2 k \downarrow} \rangle + (U' - J_H) \langle n_{A_1^2 k \uparrow} \rangle - \mu, \quad (41)$$

$$\varepsilon_{A_1^2} = \varepsilon_{t_6} + U \langle n_{A_1^2 k \downarrow} \rangle + U' \langle n_{A_1^1 k \downarrow} \rangle + (U' - J_H) \langle n_{A_1^1 k \uparrow} \rangle - \mu, \quad (42)$$

$$\varepsilon_{B_1^1} = \varepsilon_{t_6} + U \langle n_{B_1^1 k \downarrow} \rangle + U' \langle n_{B_1^2 k \downarrow} \rangle + (U' - J_H) \langle n_{B_1^2 k \uparrow} \rangle - \mu, \quad (43)$$

$$\varepsilon_{B_1^2} = \varepsilon_{t_6} + U \langle n_{B_1^2 k \downarrow} \rangle + U' \langle n_{B_1^2 k \downarrow} \rangle + (U' - J_H) \langle n_{B_1^2 k \uparrow} \rangle - \mu. \quad (44)$$

According to the itinerant picture, the interactions between two sets of pockets give rise to a SDW order at the wave vector connecting them with $Q_x = (\pi, 0)$ or $Q_y = (0, \pi)$. For example, as choosing the ordering vector Q_x , the spin configuration has antiparallel spins *along the X'-direction* and parallel spins along the Y'-direction [35]. The antiferromagnetism causes the gapless structure along the X'-direction, and the ferromagnetism opens a gap along the Y'-direction, as shown in **Figure 4(a)**. There are four pockets centered at the Γ point, and two pockets along the $\Gamma - Y'$ direction are inequivalent to other two pockets along the $\Gamma - X'$ direction. The C_2 symmetry of the Fermi surface resulting from the SDW gap is shown in **Figure 4(b)**.

In the nematic state, the antiparallel spins are along both the X'' and Y'' directions. The nematic unit cell is oriented at a 45° with respect to the nonmagnetic unit cell. The nematic Brillouin zone is also a square oriented at a 45° angle with respect to the crystal Brillouin zone. Since the antiferromagnetism is along both the X'' and Y'' directions, *there is no gap in the band structure*. In addition, as $M_1 < M_2$, the bands along the Y'' direction are lifted higher and cause the bands to be asymmetric with respect to the Γ point. The asymmetric bands result in deformed Fermi surfaces near the Γ point. As shown in **Figure 5(a)**, the blue curve in the band structure forms an elliptic hole-pocket Fermi surface. Furthermore, the elliptic Fermi surface results from the unequal contribution of two orbitals d_{xz} and d_{yz} . The mechanism behind the fluctuations of d_{xz} and d_{yz} orbitals can be understood from an extended RPA approach where d_{xz} , d_{yz} , and d_{xy} orbitals equally contribute to the SDW instability, and in particular the d_{xy} orbital plays a strong role in the nematic instability [30]. The nematic instability breaks the degeneracy of two orbitals d_{xz} and d_{yz} and causes the unequal charge distributions $n_{xz}(k)$ and $n_{yz}(k)$. The C_2 -symmetry of the Fermi surface results from the broken degeneracy of two orbitals d_{xz} and d_{yz} (blue and red curves in **Figure 5(b)**).

Recently, Qureshi et al. [53], Wang et al. [54], Steffens et al. [55], and Luo et al. [56] pointed out that in-plane spin excitations exhibit a large gap and indicating that the spin anisotropy is caused by the contribution of itinerant electrons and the topology of Fermi surface. These experiments indicate that the elliptic spin fluctuations at low energy in iron pnictides are mostly caused by the anisotropic damping

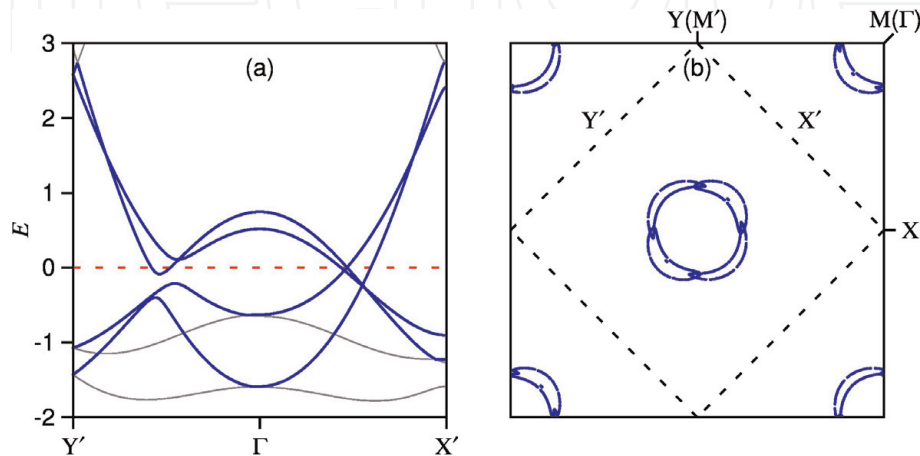


Figure 4. (color online) (a) and (b) are, respectively, the band structure and the Fermi surface in the stripe SDW state. The Fermi energy (red dashed line) corresponds to the electron filling $n = 2.04$. X' and Y' indicate the magnetic Brillouin zone of the stripe SDW state.

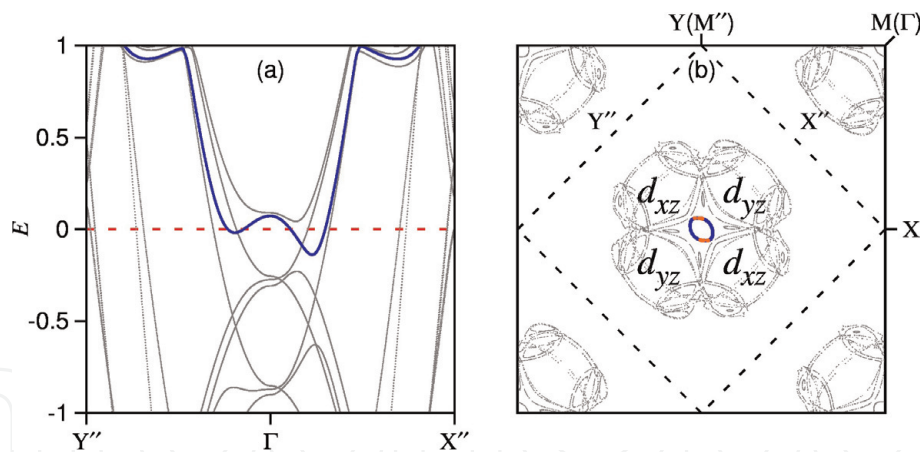


Figure 5. (color online) (a) and (b) are, respectively, the band structure and the Fermi surface in the nematic state. The asymmetric band (blue color) is responsible for the elliptic Fermi surface around the Γ point. The blue and red solid curves represent the major contributions from the orbitals d_{xz} and d_{yz} , respectively. The chemical potential is chosen as the electron filling $n = 2.1$. X' , and Y' indicate the magnetic Brillouin zone of the nematic state.

of spin waves within FeAs plane and the topology of Fermi surface. The degeneracy of orbitals will introduce the single-ion anisotropy in spin fluctuations.

3. Visualize nematicity in a lattice

To visualize the nematicity in a lattice, we self-consistently solve the Bogoliubov-de Gennes (BdG) equations for the nematic state in a two-dimensional square lattice:

$$\sum_{jv} \begin{pmatrix} h_{ijuv\uparrow} & \Delta_{ijuv} \\ \Delta_{ijuv}^* & h_{ijuv\downarrow}^* \end{pmatrix} \begin{pmatrix} u_{jv\uparrow}^n \\ v_{jv\downarrow}^n \end{pmatrix} = E_n \begin{pmatrix} u_{iu\uparrow}^n \\ v_{iu\downarrow}^n \end{pmatrix}, \quad (45)$$

where

$$h_{ij\alpha\alpha} = t_{ij\alpha\alpha} + \{-\mu + U\langle n_{iu\beta} \rangle + U'\langle n_{iv\alpha} \rangle + (U' - J_H)\langle n_{iv\beta} \rangle\} \delta_{ij}, \quad (46)$$

and $U' = U - 2J_H$. The self-consistency conditions are

$$\langle n_{iu\uparrow} \rangle = \sum_n |u_{iu\uparrow}^n|^2 f(E_n), \quad (47)$$

$$\langle n_{iu\downarrow} \rangle = \sum_n |v_{iu\downarrow}^n|^2 f(1 - E_n), \quad (48)$$

$$\Delta_{ijuu} = \frac{V}{2} \sum_n u_{iu\uparrow}^n v_{iu\downarrow}^{n*} \tanh\left(\frac{\beta E_n}{2}\right). \quad (49)$$

Here, $f(E_n)$ is the Fermi distribution function.

In **Figure 6**, we show the magnetic configuration in the coexisting state of the nematic order and SC. To view the detail of the structure, the slided profile along the peaks along the x- or y-direction is made (as shown on the sides of M_i in **Figure 6**). There are two sinusoidally modulated magnetizations on each panel. The warm color and cold color modulations represent the spin-up modulation and the spin-down modulation, respectively. The amplitude of each modulation on the left and right panels corresponds to the value of M_1 and M_2 . On the left panel,

we have $M_1 \cos(q_y \cdot r_i) = 0.04 \cos(\frac{2\pi r_i}{28a})$, and on the right panel, we have $M_2 \cos(q_x \cdot r_i) = 0.06 \sin(\frac{2\pi r_i}{28a})$. Both modulations have the same period $28a$. Since $M_1 < M_2$, the configuration is orthorhombic and breaks the 90° rotational symmetry.

Figure 7 shows the Fourier transformation of the spatial configuration of the nematic fluctuations. Two peaks appearing at $(\pm\pi, 0)$ correspond to the ordering vector Q_x and two peaks exhibiting at $(0, \pm\pi)$ correspond to the ordering vector Q_y . We found that the intensities of peaks associated with the ordering vector Q_x are greater than peaks associated with the ordering vector Q_y , which is due to the unequal value of M_1 and M_2 . The intensities of two peaks along the $k_x(k_y)$ -direction have the same magnitude indicating $\langle\Delta_x\rangle = \langle\Delta_y\rangle = 0$. Moreover, the

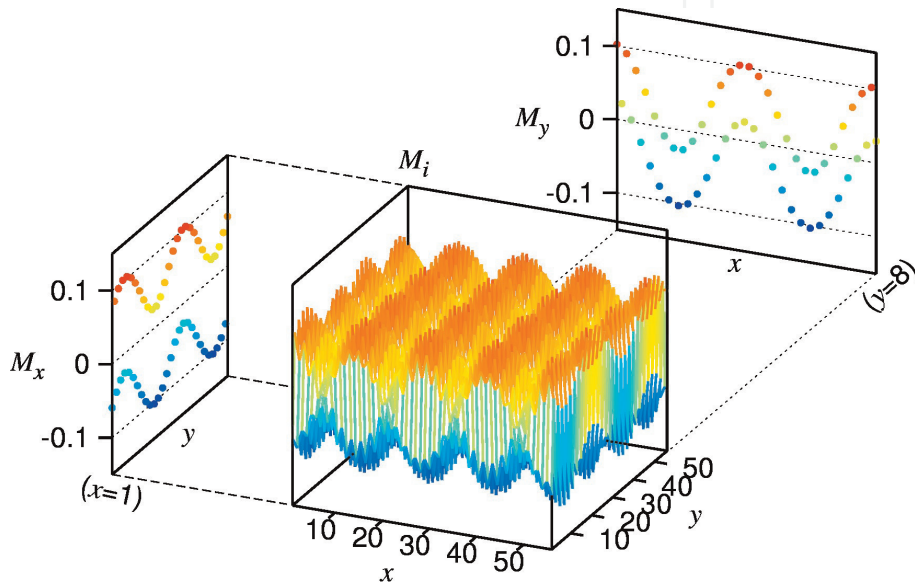


Figure 6. (color online) the real space configurations of the magnetization M_i are plotted on a 56×56 square lattice. The left and the right panels are the sliced profile along the peaks along the y - and x -directions, respectively. Two curves are shown in both panels. The upper and lower curves represent the spin-up and spin-down configurations, respectively.

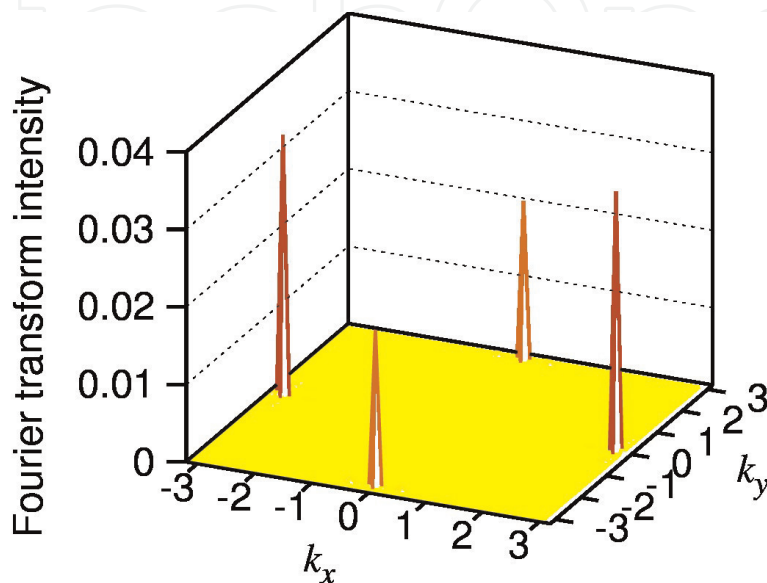


Figure 7. (color online) the Fourier transformation of the 56×56 spatial magnetic configuration.

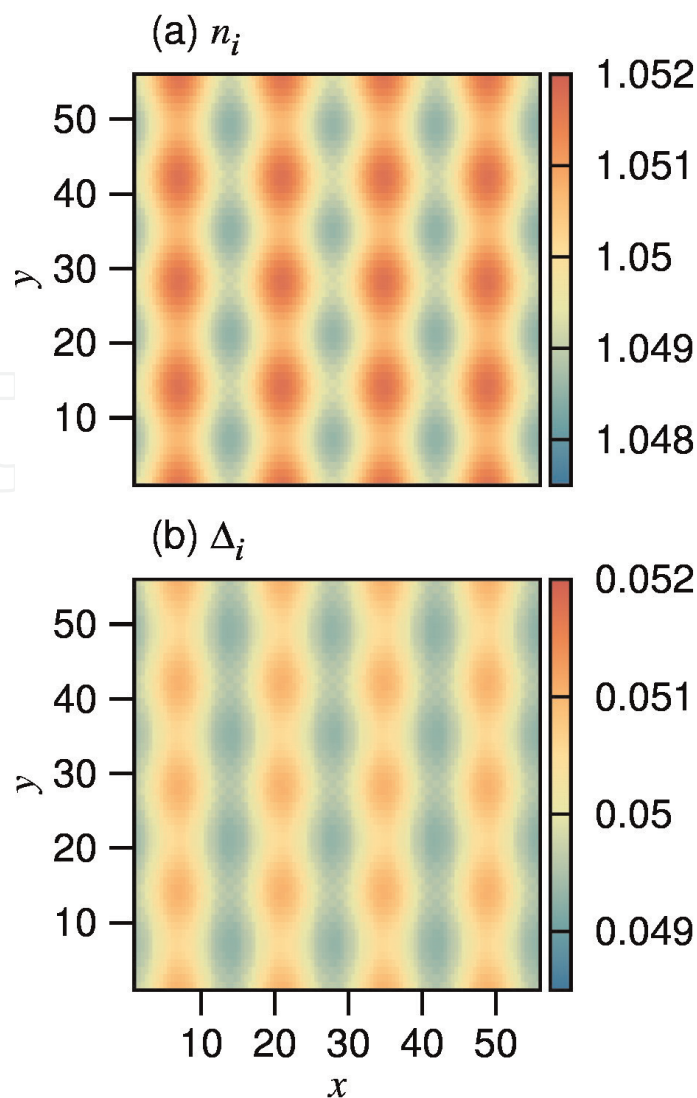


Figure 8. (color online) (a) the spatial configuration of the electronic charge density n_i . (b) the spatial configuration of the s^{+-} -wave superconducting order parameter Δ_i .

nonequivalence of the intensities between the k_x - and k_y -directions indicates $\langle \Delta_y^2 \rangle > \langle \Delta_x^2 \rangle$. Therefore, the modulated antiparallel spin configuration is the nematic state. These features are preserved even as the SC order is equal to zero. This result is in agreement with the neutron scattering experiments [3, 10].

We further illustrate the electronic charge density $n_i = (n_{i\uparrow} + n_{i\downarrow})$ and the s^{+-} -wave SC order parameter Δ_i as shown in **Figure 8(a)**, **(b)**. Particularly, the nematicity of the spin order induces a modulated charge density wave (CDW) which does not occur in the stripe SDW state. The CDW consists of crisscrossed horizontal and vertical stripes. The amplitudes of the vertical stripes are larger than the horizontal stripes. Therefore, the CDW forms a checked pattern, instead of a checkerboard pattern. The stripes on both x - and y - directions have the same period $14a$ which is the half period of the magnetization.

Moreover, although the checked pattern of the CDW is twofold symmetry, the CDW exhibits a $d_{x^2-y^2}$ -symmetry, instead of a d_{xy} -symmetry (diagonal stripes crisscrossed pattern), form factor density wave. The space configuration of the SC order parameter Δ_i shows the same features as the CDW order, as shown in **Figure 8(b)**.

4. The local density of states

The local density of states (LDOS) proportional to the differential tunneling conductance as measured by STM is expressed as

$$\rho_i(E) = -\frac{1}{N_x N_y} \sum_{nu} \left[|u_{iu\uparrow}^n|^2 f'(E_n - E) + |v_{iu\downarrow}^n|^2 f'(E_n + E) \right], \quad (50)$$

where $N_x \times N_y = 24 \times 24$ is the size of supercells.

In the striped SDW state, spins are parallel in the y-direction and antiparallel in the x-direction and cause the gap and gapless features in the band structure, respectively. The SDW gap shifts toward negative energy, and the coherence peak at the negative energy is pushed outside the SDW gap and enhanced. The coherence peak at the positive energy is moved inside the SDW gap and suppressed. This is a prominent feature caused by the magnetic SDW order that the intensities of superconducting coherence peaks are obvious asymmetry (as shown in **Figure 9(a)**) [57].

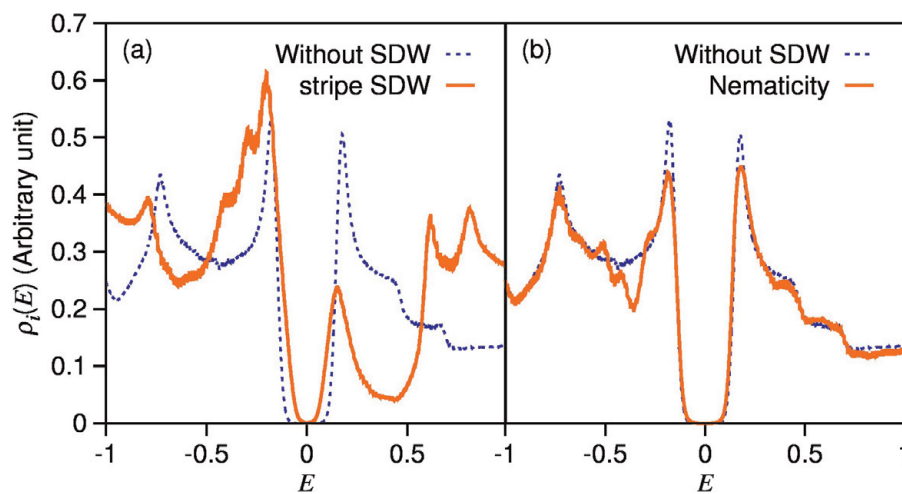


Figure 9. (color online) the LDOS in the (a) stripe SDW state and (b) nematic state. The dashed (blue) line represents the LDOS without magnetization ($M_i = 0$).

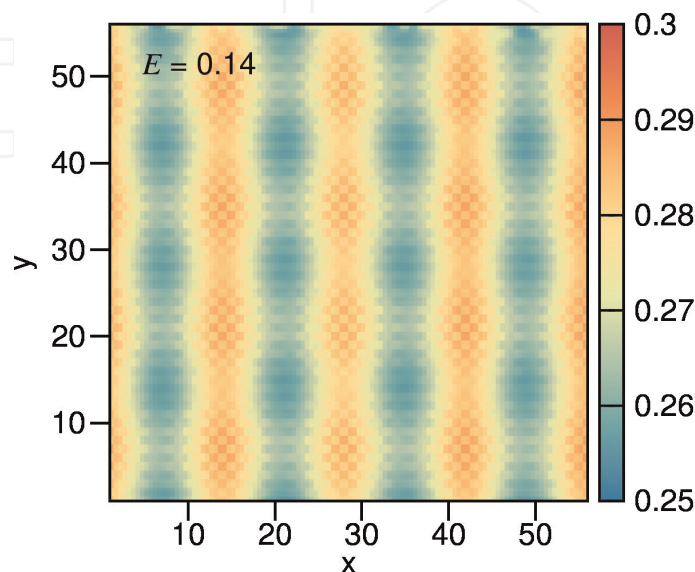


Figure 10. (Color online) The LDOS map at $E = 0.14$ with $M_i \neq 0$.

In the nematic state, spins are antiparallel in the x- and y-directions leading to a gapless feature in the band structure. The superconducting gap is the only gap that appears in the LDOS. Moreover, comparing to the state without SDW, the competition between the nematic order and the superconducting order causes the slightly suppression of the coherence peaks. The feature of the suppression results in a dip at the negative energy outside the coherence peaks (as shown in **Figure 9(b)**).

Furthermore, **Figure 10** displays a spatial distribution of LDOS, also known as LDOS map, at $E = 0.14$. The LDOS map shows the same features as the charge density distribution at the energy within the coherence peaks. The LDOS map exhibits a checked pattern, twofold symmetric configuration, and $d_{x^2-y^2}$ -symmetry form factor density wave. These features have not yet been reported by STM experiments.

It is worth to note that STM measurements by Chuang et al. [5] and Allan [58] reported that the dimension of the electronic nanostructure is around $8a$ and the nanostructure aligns in a unidirectional fashion. The highly twofold symmetric structure of the QPI patterns is represented by using the Fourier transformation of the STS imaging. Moreover, in cuprate, the more advanced measurement of the atomic-scale electronic structure has shown a d-wavelike symmetry form factor density wave [59, 60]. There are four peaks that appear around the center of the momentum space in the QPI patterns. Such an atomic-scale feature in cuprates has not yet been reported in iron pnictides and in the nematic state.

5. Phase diagram

To further verify the spin configuration of the nematic order, a phase diagram is presented in **Figure 11**. In the phase diagram, the stripe SDW order, nematic order, and s^{+-} -wave superconducting order as a function of doping are obtained from the self-consistent calculation to solve the BdG equations.

In the hole-doped region, the magnetization exhibits the stripe SDW order and drops dramatically around $n = 1.85$ and vanishes at $n = 1.80$. In the meantime, the s^{+-} -wave superconducting order reaches its maximal value at $n = 1.85$ and then gradually decreases.

In the electron-doped region, the stripe SDW order (green curve) has its maximal value at $n = 2.00$, then rapidly diminishes in a small region of doping, and finally reaches zero at $n = 2.09$. The superconductivity (blue curve) swiftly increases in a small region from $n = 2.02$ to $n = 2.04$, then reaches its maximal

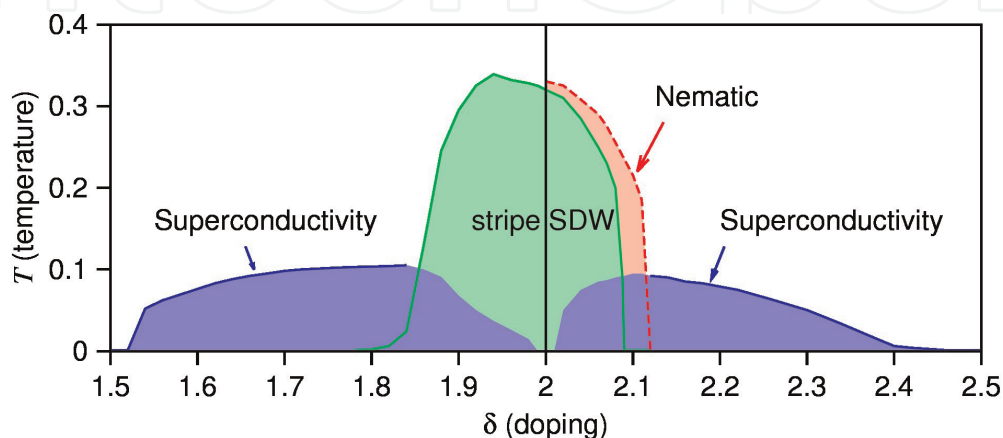


Figure 11. (color online) the phase diagram of the stripe SDW order (blue), nematic order (green), and superconducting order (red) as a function of doping.

value at $n = 2.10$, and finally gradually decreases to almost zero around $n = 2.40$. The nematic state (red region) is in a small region next to the stripe SDW where the nematic transition line (red dashed curve) tracks closely the stripe SDW transition line. The nematic order is favored to appear in the electron-doped regime, but not the hole-doped regime.

There are two regions where the stripe SDW coexist with the SC and the nematic order coexists with the SC. In the region where the stripe SDW coexist with the SC, the magnetic structure is an orthorhombic uniaxial stripe state. The ordering vector is either Q_x or Q_y implying $\langle \Delta_x \rangle = 0$ or $\langle \Delta_y \rangle = 0$. In the region where the nematic order coexists with the SC, the magnetic structure is a crisscrossed stripe state with twofold symmetry. The ordering vectors are Q_x and Q_y associated with two modulating vectors q_x and q_y implying $\langle \Delta_x \rangle = \langle \Delta_y \rangle = 0$ and $\langle \Delta_x^2 - \Delta_y^2 \rangle \neq 0$ [61].

It is worth to note that the phase diagram of the electron-doped region is consistent with Figure 1.3 of Kuo's thesis on $\text{Ba}(\text{Fe}_{1-x}\text{Co}_x\text{As})_2$ [62]. Both figures show the same behavior of the nematic phase. Near the optimally doped region under the superconducting dome, it is mentioned that the long-range nematic order coexists with the superconductivity. However, such results still have not been reported from experiments. In addition, the magnetoresistivity of $\text{Ba}_{0.5}\text{K}_{0.5}\text{Fe}_2\text{As}_2$ reported a nematic superconducting state recently and suggested that the hole-doped superconductor is the mixture of s -wave and d -wave superconducting orders [63]. These results provide a different path to further researches to understand the mechanism of the nematic state in the superconductivity.

6. Conclusions

The two-orbital Hamiltonian used in the iron-based superconductors has always been questioned for its validity. Many studies have approved that a lot of phenomena are attributed to d_{xz} and d_{yz} orbitals. In particular, d_{xz} and d_{yz} orbitals are responsible for the SDW instability.

The stripe SDW order opens a gap in the band structure and deforms the Fermi surface. However, the band structure of the nematic order is gapless, and the Fermi surface is deformed to an ellipse. The mechanism can be understood from the instability of SDW. The nematic order has visualized as a checked pattern formed by a crisscrossed modulated horizontal and vertical stripes. The inequivalent strengths of the horizontal and vertical stripes break the degeneracy of two orbitals d_{xz} and d_{yz} and cause an elliptic Fermi surface. The Fourier transformation of the orthorhombic structure of the magnetization shows two uneven pairs of peaks at $(\pm\pi, 0)$ and $(0, \pm\pi)$. Moreover, the LDOS map shows a $d_{x^2-y^2}$ -symmetry form factor density wave.

Finally, the nematic order is favored to exist in the electron-doped regime, but not the hole-doped regime.

Acknowledgements

HYC was supported by MOST of Taiwan under Grant MOST 107-2112-M-003-002 and National Center for Theoretical Science of Taiwan.

IntechOpen

IntechOpen

Author details

Hong-Yi Chen

Department of Physics, National Taiwan Normal University, Taipei, Taiwan

*Address all correspondence to: hongyi@ntnu.edu.tw

IntechOpen

© 2020 The Author(s). Licensee IntechOpen. This chapter is distributed under the terms of the Creative Commons Attribution License (<http://creativecommons.org/licenses/by/3.0>), which permits unrestricted use, distribution, and reproduction in any medium, provided the original work is properly cited. 

References

- [1] Christianson AD, Goremychkin EA, Osborn R, Rosenkranz S, Lumsden MD, Malliakas CD, et al. Unconventional superconductivity in $\text{Ba}_{0.6}\text{K}_{0.4}\text{Fe}_2\text{As}_2$ from inelastic neutron scattering. *Nature*. 2008;**456**:930
- [2] Séamus Davis JC, Lee D-H. Concepts relating magnetic interactions, intertwined electronic orders, and strongly correlated superconductivity. *PNAS*. 2013;**110**:17623
- [3] Zhao J, Adroja DT, Yao D-X, Bewley R, Li S, Wang XF, et al. Spin waves and magnetic exchange interactions in CaFe_2As_2 . *Nature Physics*. 2009;**5**:555
- [4] Yi M, Donghui L, Chu J-H, Analytis JG, Sorini AP, Kemper AF, et al. Symmetry-breaking orbital anisotropy observed for detwinned $\text{Ba}(\text{Fe}_{1-x}\text{Co}_x)_2\text{As}_2$ above the spin density wave transition. *PNAS*. 2011;**108**:6878
- [5] Chuang T-M, Allan MP, Lee J, Xie Y, Ni N, Bud'ko SL, et al. Nematic electronic structure in the “Parent” State of the iron-based superconductor $\text{Ca}(\text{Fe}_{1-x}\text{Co}_x)_2\text{As}_2$. *Science*. 2010;**327**:181
- [6] Chu J-H, Analytis JG, De Greve K, McMahon PL, Islam Z, Yamamoto Y, et al. In-plane resistivity anisotropy in an underdoped iron arsenide superconductor. *Science*. 2010;**329**:824
- [7] Chu J-H, Analytis JG, Press D, De Greve K, Ladd TD, Yamamoto Y, et al. In-plane electronic anisotropy in underdoped $\text{Ba}(\text{Fe}_{1-x}\text{Co}_x)_2\text{As}_2$ revealed by partial detwinning in a magnetic field. *Physical Review B*. 2010;**81**:214502
- [8] Shimojima T, Ishizaka K, Ishida Y, Katayama N, Ohgushi K, Kiss T, et al. Orbital-dependent modifications of electronic structure across the Magnetostructural transition in BaFe_2As_2 . *Physical Review Letters*. 2010;**104**:057002
- [9] Tanatar MA, Blomberg EC, Kreyssig A, Kim MG, Ni N, Thaler A, et al. Uniaxial-strain mechanical detwinning of CaFe_2As_2 and BaFe_2As_2 crystals: Optical and transport study. *Physical Review B*. 2010;**81**:184508
- [10] Harriger LW, Luo HQ, Liu MS, Frost C, Hu JP, Norman MR, et al. Nematic spin fluid in the tetragonal phase of BaFe_2As_2 . *Physical Review B*. 2011;**84**:054544
- [11] Nakajima M, Liang T, Ishida S, Tomioka Y, Kihou K, Lee CH, et al. Unprecedented anisotropic metallic state in undoped iron arsenide BaFe_2As_2 revealed by optical spectroscopy. *PNAS*. 2011;**108**:12238
- [12] Kuo H-H, Chu J-H, Riggs SC, Yu L, McMahon PL, De Greve K, et al. Possible origin of the nonmonotonic doping dependence of the in-plane resistivity anisotropy of $\text{Ba}(\text{Fe}_{1-x}\text{T}_x)_2\text{As}_2$ ($\text{T}=\text{Co}, \text{Ni}$ and Cu). *Physical Review B*. 2011;**84**:054540
- [13] Kasahara S, Shi HJ, Hashimoto K, Tonegawa S, Mizukami Y, Shibauchi T, et al. Electronic nematicity above the structural and superconducting transition in $\text{BaFe}_2(\text{As}_{1-x}\text{P}_x)_2$. *Nature*. 2012;**486**:382
- [14] Chu J-H, Kuo H-H, Analytis JG, Fisher IR. Divergent nematic susceptibility in an iron arsenide superconductor. *Science*. 2012;**337**:710
- [15] Fernandes RM, Böhmer AE, Meingast C, Schmalian J. Scaling between magnetic and lattice fluctuations in iron pnictide superconductors. *Physical Review Letters*. 2013;**111**:137001

- [16] Blomberg EC, Tanatar MA, Fernandes RF, Mazin II, Shen B, Wen H-H, et al. Sign-reversal of the in-plane resistivity anisotropy in hole-doped iron pnictides. *Nature Communications*. 2013;**4**:1914
- [17] Mirri C, Dusza A, Bastelberger S, Chu J-H, Kuo H-H, Fisher IR, et al. Nematic-driven anisotropic electronic properties of underdoped detwinned Ba (Fe_{1-x}Cox)₂As₂ revealed by optical spectroscopy. *Physical Review B*. 2014;**90**:155125
- [18] Fernandes RM, Chubukov AV, Schmalian J. What drives nematic order in iron-based superconductors? *Nature Physics*. 2014;**10**:97
- [19] Lv W, Phillips P. Orbital and magnetically induced anisotropy in iron-based superconductors. *Physical Review B*. 2011;**84**:174512
- [20] Lee W-C, Phillips PW. Non-Fermi liquid due to orbital fluctuations in iron pnictide superconductors. *Physical Review B*. 2012;**86**:245113
- [21] Arham HZ, Hunt CR, Park WK, Gillett J, Das SD, Sebastian SE, et al. Detection of orbital fluctuations above the structural transition temperature in the iron pnictides and chalcogenides. *Physical Review B*. 2012;**85**:214515
- [22] Stanev V, Littlewood PB. Nematicity driven by hybridization in iron-based superconductors. *Physical Review B*. 2013;**87**:161122(R)
- [23] Yamase H, Zeyher R. Superconductivity from orbital nematic fluctuations. *Physical Review B*. 2013;**88**:180502(R)
- [24] Fernandes RM, Chubukov AV, Knolle J, Eremin I, Schmalian J. Preemptive nematic order, pseudogap, and orbital order in the iron pnictides. *Physical Review B*. 2012;**85**:024534
- [25] Hu JP, Xu C. Nematic orders in Iron-based superconductors. *Physica C*. 2012;**481**:215
- [26] Fernandes RM, Schmalian J. Manifestations of nematic degrees of freedom in the magnetic, elastic, and superconducting properties of the iron pnictides. *Superconductor Science and Technology*. 2012;**25**:084005
- [27] Avci S, Chmaissem O, Allred JM, Rosenkranz S, Eremin I, Chubukov AV, et al. Magnetically driven suppression of nematic order in an iron-based superconductor. *Nature Communications*. 2014;**5**:3845
- [28] Xingye L, Park JT, Zhang R, Luo H, Nevidomskyy AH, Si Q, et al. Nematic spin correlations in the tetragonal state of uniaxial-strained BaFe_{2-x}Ni_xAs₂. *Science*. 2014;**345**:657
- [29] Zhang W, Park JT, Lu X, Wei Y, Ma X, Hao L, et al. Effect of Nematic order on the low-energy spin fluctuations in Detwinned BaFe_{1.935}Ni_{0.065}As₂. *Physical Review Letters*. 2016;**117**:227003
- [30] Christensen MH, Kang J, Andersen BM, Fernandes RM. Spin-driven nematic instability of the multiorbital Hubbard model: Application to iron-based superconductors. *Physical Review B*. 2016;**93**:085136
- [31] Khalyavin DD, Lovesey SW, Maneul P, Kruger F, Rosenkranz S, Allred JM, et al. Symmetry of reentrant tetragonal phase in Ba_{1-x}NaxFe₂As₂: Magnetic versus orbital ordering mechanism. *Physical Review B*. 2014;**90**:174511
- [32] Böhmer AE, Hardy F, Wang L, Wolf T, Schweiss P, Meingast C. Superconductivity-induced re-entrance of the orthorhombic distortion in Ba_{1-x}K_xFe₂As₂. *Nature Communications*. 2015;**6**:7911

- [33] Wang X, Kang J, Fernandes RM. Magnetic order without tetragonal-symmetry-breaking in iron arsenides: Microscopic mechanism and spin-wave spectrum. *Physical Review B*. 2015;**91**:024401
- [34] Gastiasoro MN, Andersen BM. Competing magnetic double-Q phases and superconductivity-induced reentrance of C2 magnetic stripe order in iron pnictides. *Physical Review B*. 2015;**92**:140506(R)
- [35] Pan L, Li J, Tai Y-Y, Graf MJ, Zhu J-X, Ting CS. Evolution of the Fermi surface topology in doped 122 iron pnictides. *Physical Review B*. 2013;**88**:214510
- [36] Zhao YY, Li B, Li W, Chen H-Y, Bassler KE, Ting CS. Effects of single- and multi-substituted Zn ions in doped 122-type iron-based superconductors. *Physical Review B*. 2016;**93**:144510
- [37] Gao Y, Huang H-X, Chen C, Ting CS, Su W-P. Model of vortex states in hole-doped Iron-Pnictide superconductors. *Physical Review Letters*. 2011;**106**:027004
- [38] Kuroki K, Onari S, Arita R, Usui H, Tanaka Y, Kontani H, et al. Unconventional pairing originating from the disconnected Fermi surfaces of superconducting $\text{LaFeAsO}_{1-x}\text{F}_x$. *Physical Review Letters*. 2008;**101**:087004
- [39] Lee PA, Wen X-G. Spin-triplet p-wave pairing in a three-orbital model for iron pnictide superconductors. *Physical Review B*. 2008;**78**:144517
- [40] Daghofer M, Nicholson A, Moreo A, Dagotto E. Three orbital model for the iron-based superconductors. *Physical Review B*. 2010;**81**:014511
- [41] Vorontsov AB, Vavilov MG, Chubukov AV. Interplay between magnetism and superconductivity in the iron pnictides. *Physical Review B*. 2009;**79**:060508(R)
- [42] Maiti S, Fernandes RM, Chubukov AV. Gap nodes induced by coexistence with antiferromagnetism in iron-based superconductors. *Physical Review B*. 2012;**85**:144527
- [43] Parker D, Vavilov MG, Chubukov AV, Mazin II. Coexistence of superconductivity and a spin-density wave in pnictide superconductors: Gap symmetry and nodal lines. *Physical Review B*. 2009;**80**:100508
- [44] Beaird R, Vekhter I, Zhu J-X. Impurity states in multiband s-wave superconductors: Analysis of iron pnictides. *Physical Review B*. 2012;**86**:140507(R)
- [45] Maisuradze A, Yaouanc A. Magnetic form factor, field map, and field distribution for a BCS type-II superconductor near its $B_{c2}(T)$ phase boundary. *Physical Review B*. 2013;**87**:134508
- [46] Gastiasoro MN, Hirschfeld PJ, Andersen BM. Impurity states and cooperative magnetic order in Fe-based superconductors. *Physical Review B*. 2013;**88**:220509(R)
- [47] Zhang D. Nonmagnetic impurity resonances as a signature of sign-reversal pairing in FeAs-based superconductors. *Physical Review Letters*. 2009;**103**:186402
- [48] Tai YY, Zhu J-X, Matthias JG, Ting CS. Calculated phase diagram of doped BaFe_2As_2 superconductor in a C4-symmetry breaking model. *Europhysics Letters*. 2013;**103**:67001
- [49] Castellani C, Natoli CR, Ranninger J. Magnetic structure of V_2O_3 in the insulating phase. *Physical Review B*. 1978;**18**:4945

- [50] Ghaemi P, Wang F, Vishwanath A. Andreev bound states as a phase-sensitive probe of the pairing symmetry of the iron pnictide superconductors. *Physical Review Letters*. 2009;**102**:157002
- [51] Zhang X, Oh YS, Liu Y, Yan L, Kim KH, Greene RL, et al. Observation of the Josephson effect in Pb/Ba $_{1-x}$ KxFe $_2$ As $_2$ single crystal junctions. *Physical Review Letters*. 2009;**102**:147002
- [52] Seo K, Bernevig BA, Hu J. Pairing symmetry in a two-orbital exchange coupling model of Oxypnictides. *Physical Review Letters*. 2008;**101**:206404
- [53] Qureshi N, Steffens P, Wurmehl S, Aswartham S, Büchner B, Braden M. Local magnetic anisotropy in BaFe $_2$ As $_2$: A polarized inelastic neutron scattering study. *Physical Review B*. 2012;**86**:060410(R)
- [54] Wang C, Zhang R, Wang F, Luo H, Regnault LP, Dai P, et al. Longitudinal spin excitations and magnetic anisotropy in Antiferromagnetically ordered BaFe $_2$ As $_2$. *Physical Review X*. 2013;**3**:041036
- [55] Steffens P, Lee CH, Qureshi N, Kihou K, Iyo A, Eisaki H, et al. Splitting of resonance excitations in nearly optimally doped Ba(Fe $_{0.94}$ Co $_{0.06}$) $_2$ As $_2$: An inelastic neutron scattering study with polarization analysis. *Physical Review Letters*. 2013;**110**:137001
- [56] Luo H, Wang M, Zhang C, Lu X, Regnault L-P, Zhang R, et al. Spin excitation anisotropy as a probe of orbital ordering in the paramagnetic tetragonal phase of superconducting BaFe $_{1.904}$ Ni $_{0.096}$ As $_2$. *Physical Review Letters*. 2013;**111**:107006
- [57] Pan L, Li J, Tai Y-Y, Graf MJ, Zhu J-X, Ting CS. Evolution of quasiparticle states with and without a Zn impurity in doped 122 iron pnictides. *Physical Review B*. 2014;**90**:134501
- [58] Allan MP, Chuang T-M, Masee F, Xie Y, Ni N, Bud'ko SL, et al. Anisotropic impurity states, quasiparticle scattering and nematic transport in underdoped Ca(Fe $_{1-x}$ Cox) $_2$ As $_2$. *Nature Physics*. 2013;**9**:220
- [59] Fujita K, Hamidian MH, Edkins SD, Kim CK, Kohsaka Y, Azuma M, et al. Direct phase-sensitive identification of a d-form factor density wave in underdoped cuprates. *PNAS*. 2014;**111**:E3026
- [60] Hamidian MH, Edkins SD, Kim CK, Davis JC, Mackenzie AP, Eisaki H, et al. Atomic-scale electronic structure of the cuprate d-symmetry form factor density wave state. *Nature Physics*. 2016;**12**:150
- [61] Chou C-P, Chen H-Y, Ting CS. The nematicity induced d -symmetry charge density wave in electron-doped iron-pnictide superconductors. *Physica C*. 2018;**546**:61
- [62] Kuo H-H. Electronic Nematicity in Iron-Based Superconductors [Thesis]. Stanford University; 2014
- [63] Li J, Pereira PJ, Yuan J, Lv Y-Y, Jiang M-P, Lu D, et al. Nematic superconducting state in iron pnictide superconductors. *Nature Communications*. 2017;**8**:1880